Mechanisms of fatigue fracture in short glass fibre-reinforced polymers

R. W. LANG*, J. A. MANSON, R. W. HERTZBERG
Materials Research Center, Lehigh University, Bethlehem, Pennsylvania 18015, USA

Fatigue-crack profiles and fracture surfaces of several short glass fibre-reinforced polymers were examined to gain insight into the mechanisms of cyclic damage and fatigue-crack propagation in these materials. Several distinctly different features were noted between fracture surfaces generated by stable fatigue crack growth and those produced by monotonic or unstable fracture. Among the most significant differences were the higher degree of single and multiple fibre fracture generally observed on stable fatigue-crack growth fracture surfaces, and the variations in the interfacial failure site in well-bonded systems. While the former effect is attributed to the occurrence of crack closure and the build-up of compressive stresses in the crack-tip damage zone during unloading, the differences in the interfacial failure mode are related to the adverse effect of fatigue loading on the interfacial bond strength. No features could be identified that would allow a quantitative correlation between the applied stress intensity factor level or the crack growth rates and characteristic fracture surface details.

1. Introduction

As a result of significant technological advances in processing and because of the continuous improvement in material properties, short fibre-reinforced (sfr) plastics are now being used increasingly for load-bearing components. Although many of these applications involve cyclic loading, and fatigue crack or damage growth is well recognized as a primary cause of failure in many reinforced plastics [1–3], only a limited amount of information on this subject is available [3–11]. For most systems studied so far it has been found that the fatigue-crack propagation (FCP) resistance of polymeric solids can be significantly improved by the incorporation of short fibres. On the other hand, conditions may exist under which the addition of short fibres into polymeric matrices may be detrimental to FCP resistance [3, 11]. While much of the previous work [3–11] was concerned primarily with the effects of material parameters (i.e. fibre content, fibre aspect ratio, orientation, interfacial strength) on the macroscopic FCP behaviour, a more complete understanding of the micromechanisms governing fatigue failure is necessary to optimize the fatigue properties of these materials.

Whenever a crack propagates through a material it produces a fracture surface morphology that reflects the local modes of failure. The usefulness of fractographic examinations as a tool towards a better understanding of fracture in engineering materials is, therefore, generally accepted [12, 13]. For example, a careful investigation of fracture surface details can provide significant insight into the micromechanisms and energetics of the fracture process, and hence may contribute to the development of improved materials through systematic modifications in the material's microstructure and composition. Also, important quantitative information regarding the mechanics and kinetics of the fracture process itself can be obtained in many cases, which may then be used in the failure analysis of engineering components.

The objective of this study is to describe the micromorphology and to identify characteristic details of fracture surfaces generated by stable FCP in several short glass fibre-reinforced (sgfr) thermoplastics. Several specific features are compared and contrasted with observations from fracture surfaces produced under fast fracture or monotonic loading conditions. Based on the fractographic evidence, mechanisms are proposed describing some of the important micromodes of failure in these materials during stable FCP.

2. Materials and experimental techniques

The materials and specimens examined in this investigation are identical with those used to generate FCP data reported previously [3, 6, 8, 9]; sources and characteristics of these materials are listed in Table I. The thermoplastic matrix materials include several types of nylon of various ductilities and polystyrene (PS), which is comparatively brittle. The reinforcing fibres were of the E-glass type in all cases. Because detailed information on the fibre-surface treatments was not available, the degree of fibre/matrix adhesion was classified qualitatively on the basis of fracture surface observations using the degree of fibre pull-out and the fibre surface appearance as relative measures for the interfacial bond strength.

All materials were supplied as injection-moulded plaques in either of the two geometries depicted in Fig. 1a. Specimens of the compact-type (CT) geometry
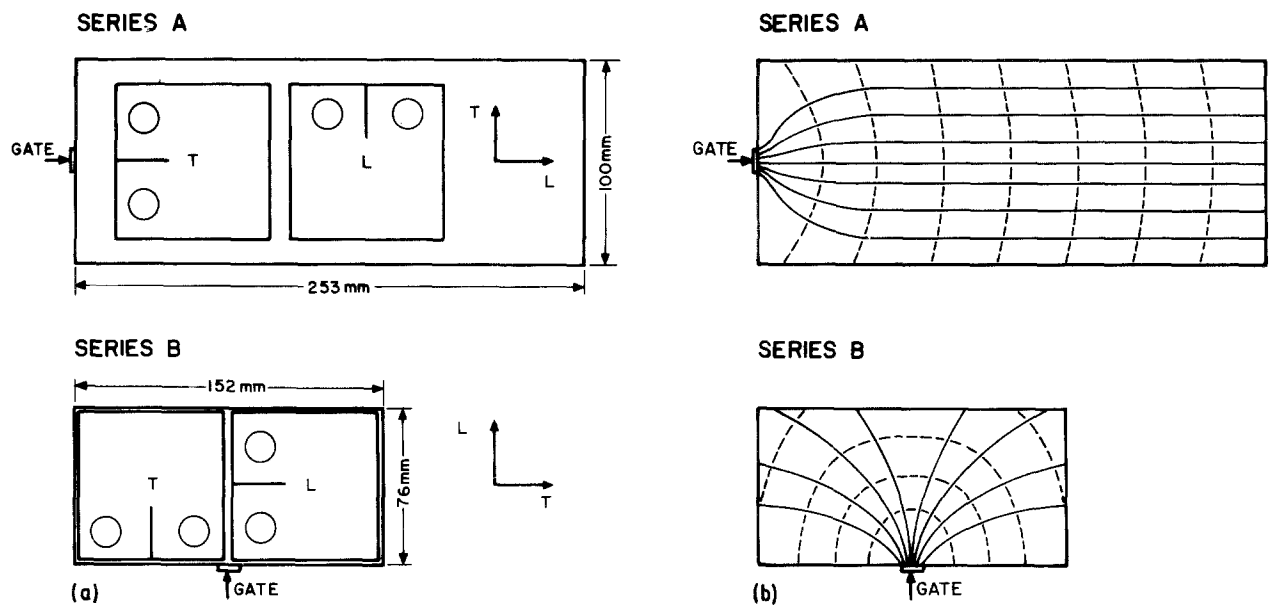
SERIES A

SERIES A

SERIES B

SERIES B

(a)

(b)

Figure 1 (a) Geometry of injection-moulded plaques and orientation of FCP specimens; T (transverse) and L (longitudinal) refer to the direction of the applied load relative to the main flow direction; (b) schematic representation of the main fibre orientations; solid and dashed lines, respectively, represent the skin and core layers of the plaques.

were cut in two different orientations so that the direction of the applied load was either longitudinal (L) or transverse (T) to the mould-fill direction. Regarding the fibre orientation in injection-moulded plaques it is well known that the main fibre orientation may vary over the plaque thickness as if the plaque consisted of several different layers [3, 6, 7, 14, 15]. Generally, a moulding will have a preferred alignment of fibres in the flow direction in the surface or skin layers, and have fibres aligned mainly transverse to the flow direction in the central or core layer. These idealized fibre-orientation distributions are based on considerations of the effects of shear flow against divergent flow [3, 6, 14, 15] and are shown schematically in Fig. 1b for the two plaque geometries.

Fatigue-crack propagation experiments were conducted in laboratory atmosphere at 24 ± 1° C, using a sinusoidal load under tension–tension load control; the cyclic frequency was 10 Hz and the minimum/ maximum load ratio, R, was 0.1. The side surfaces of some of the FCP specimens were first polished for

crack profile and crack-tip damage observations using a 1 μm diamond paste compound. The FCP tests in these cases were terminated before total specimen rupture occurred. Subsequently a wedge was introduced into the machined notch to keep the crack faces somewhat separated, and the region surrounding the crack was then cut out for microscopic observations. In addition, several precracked specimens were fractured under monotonic loading conditions at a loading rate of 185 N sec^{-1}. More detailed information on material characteristics and testing variables is available from the references listed in Table I.

All fractographic examinations were carried out using optical or scanning electron microscopy (SEM). For the latter purpose, specimens were sputter-coated with a 15 to 20 nm thick layer of gold–palladium in order to provide for efficient charge transfer. The ETEC-Autoscan scanning electron microscope was operated at an accelerating voltage of 20 kV. The crack-growth direction in all micrographs presented in this work is from left to right.

TABLE I Materials and specimen designation

Material designation*	Commercial designation*	Matrix type	Glass fibre[†] content (vol (wt)%)	Matrix ductility[‡]	Fibre–matrix adhesion	Reference
N66-18G(A)	Zytel 70G33L	nylon 66[§]	18(33)	semi-ductile	good	[6]
N66-26G(A)	Zytel 70G43L	nylon 66[§]	26(43)	semi-ductile	good	[6]
N612-25G(A)	Zytel 77G43	nylon 612	25(43)	semi-ductile	good	[6]
N66(B)	R-1000	nylon 66[¶]	–	ductile	–	[6, 8]
N66-16G(B)	RF-1006	nylon 66[¶]	16(30)	ductile	poor	[6, 8]
N66-31G(B)	RF-10010	nylon 66[¶]	31(50)	ductile	poor	[6, 8]
PS(B)	C-1000	poly(styrene)	–	brittle	–	[3, 9]
PS-18G(B)	CF-1007	poly(styrene)	18(35)	brittle	poor	[3, 9]

*Series A (duPont) and B (LNP-Corporation) supplied as end-gated and side-gated injection-moulded plaques, respectively (see Fig. 1); symbols L and T added to the material designation refer to the direction of applied load relative to the major flow direction (L-longitudinal, T-transverse).

[†] E-glass.

[‡] The classification of matrix ductility is based on fracture surface observations, and on the dynamic fracture toughness values of the unreinforced matrix which are available from the references listed.

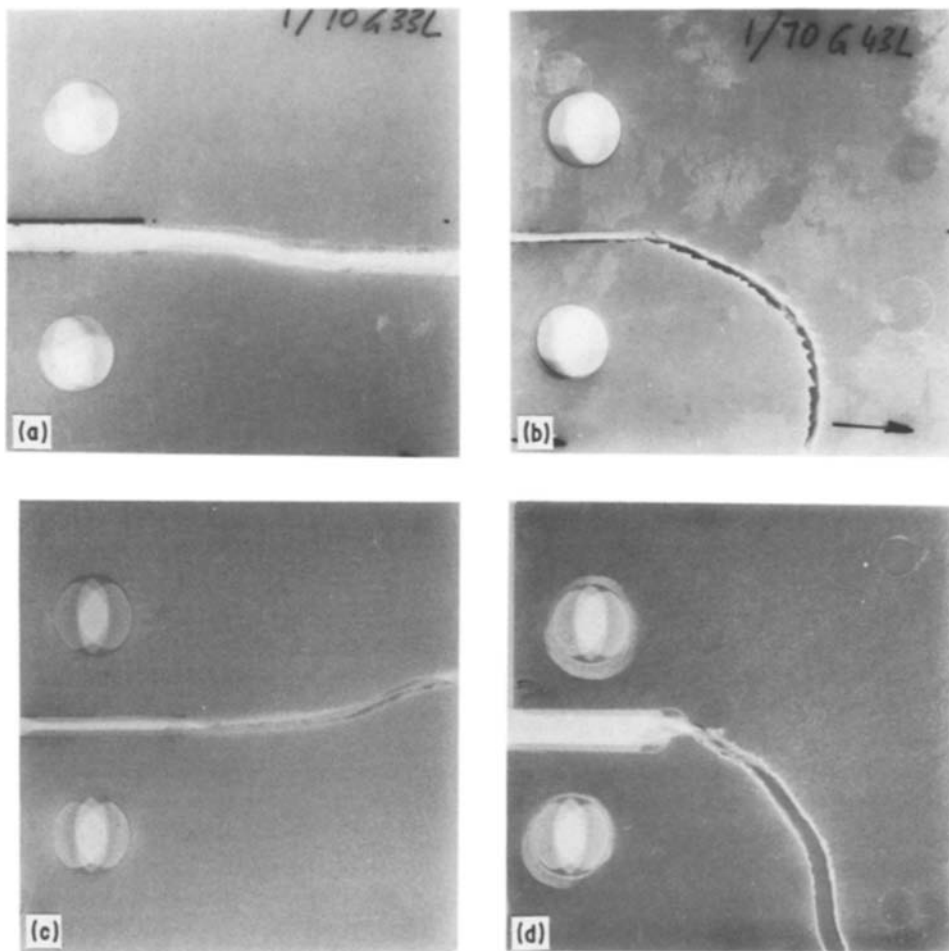[§] Dry, as-moulded (0.2 to 0.6 wt % water).

[¶] 1.7 wt % water.

Figure 2 Failed FCP specimens of (a) N66-18G(A-T); (b) N66-26G(A-T); (c) N66-16G(B-L); and (d) PS-18G(B-L).

3. Results and discussion
3.1. Macroscopic observations

Perhaps one of the most severe problems encountered in fracture and FCP experiments of short-fibre composites is related to the complexity of modes by which crack propagation may occur. For instance, while cracks were found to grow essentially in the desired plane perpendicular to the loading direction in some cases, excessive departure from this plane has been reported in others [3, 6, 9, 16]. Typical examples of failed specimens are shown in Fig. 2. Unfortunately, crack curvature as depicted in Figs 2b and d limits the applicability of conventional fracture mechanics techniques. Nevertheless, as mentioned previously [3], FCP experiments even under these circumstances may be useful in order to gain insight into the micromechanisms of fatigue failure.

Of course, any observed crack shape will reflect the path of the least resistance to crack propagation under the given loading conditions. Depending on the local fibre orientation at the crack tip, significant shear stresses may develop at the fibre/matrix interface or in the matrix itself. Thus, although it is generally true that a maximum in the driving force exists to propagate the crack in a direction perpendicular to the applied load, deviations may occur in sf-composites in the form of shear cracks that grow parallel to some predominant fibre orientation either along the fibre/matrix interface or in the adjacent matrix.

The significantly curved crack shapes shown in Figs 2b and d for N66-26G(A-T) and PS-18G(B-L),

respectively, are apparently consistent with the main fibre orientations in the centre layers of the corresponding plaques in Fig. 1b. The different crack path observations in Figs 2a and c for N66-18G(A-T) and N66-16G(B-L) (which were cut from injection-moulded plaques of identical geometry and in the same orientation as those in Figs 2b and d, respectively), on the other hand, indicate that fibre content and aspect ratio, the nature of the matrix (i.e. matrix ductility), and the degree of interfacial adhesion can be of importance.

The tendency for the development of crack curvature will depend on both the fibre orientation distribution ahead of the crack tip, and the local stress/strength ratio for fibre fracture or pull-out relative to this ratio for shear failure parallel to the main fibre orientation. According to Figs 2a and b, shear crack propagation parallel to some predominant fibre orientation appears to be favoured by an increase in fibre content due to the associated increase in crack-propagation resistance for cracks growing perpendicular (or at high angles) to the fibres. Crack curvature is also encountered more frequently with brittle matrices (Figs 2c and d) possibly because these facilitate shear crack growth parallel to the fibres.

On the macroscopic level there may or may not be a clear difference in the fracture surface appearance between the stable FCP region and the final fast fracture region associated with the last loading cycle. As with unreinforced crystalline polymers [13], the fracture surfaces of most of the nylon composites clearly
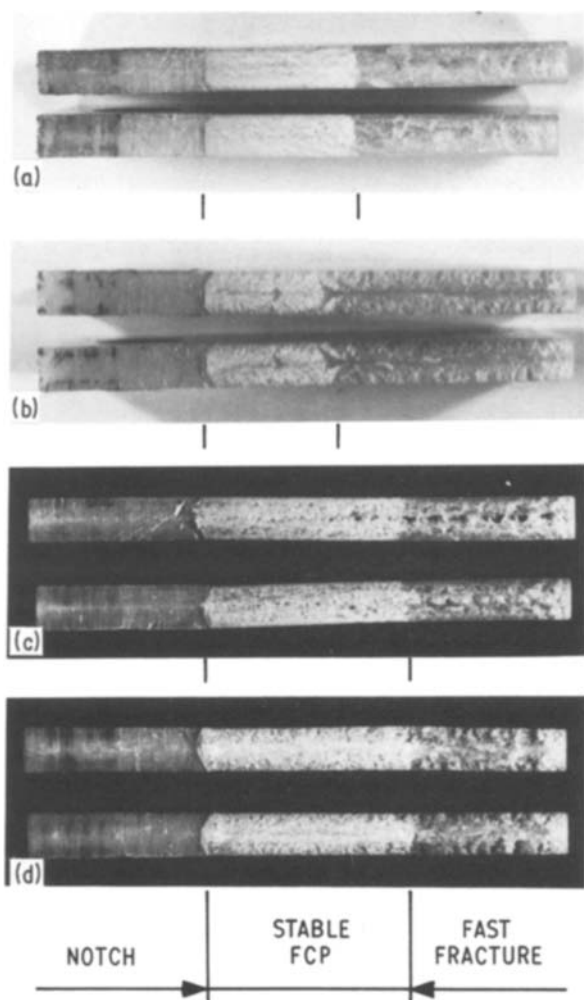
Figure 3 Macroscopic fracture surface appearance of (a) N66-18G(A-T); (b) N66-18G(A-L); (c) N612-25G(A-T); and (d) N612-25G(A-L).

example, the magnified view of the transition from stable fatigue crack growth to final fast fracture for N66-18G(A-T) in Fig. 4a shows a significantly higher degree of roughness in the core layer of the fast fracture region. Similar effects can be seen in Fig. 4b for the side surface appearance of the crack path in N66-18G(A-L). The high degree of roughness in the centre and surface layers, respectively, in the fast fracture regions of the L- and T-specimens of the materials of Series A is characteristic of crack growth in a fibre agglomeration avoidance mode whenever fibres are oriented at high angles to the main crack plane. It should be noted that these observations regarding the fast fracture regions are in good agreement with the schematic patterns of the fibre orientation distributions depicted in Fig. 1b, and findings by others from fracture toughness tests [16, 17]. The comparatively flatter appearance of the fracture surfaces in the stable FCP region, on the other hand, serves as a first indication for some differences between the fracture modes during stable FCP and fast (unstable) or monotonic fracture.

3.2. Microscopic observations
3.2.1. Examination for quantifiable fracture-surface details

Concerning fatigue fractures, many distinctive fracture-surface features and markings have been reported for metals and also for unreinforced polymers [12, 13]. These markings include certain arrest lines (often referred to as "clam shell markings" or "beach markings") that are generated by periods of fatigue crack growth, and "true" fatigue striations which correspond to crack tip positions after individual load excursions. The existence of yet another set of markings, the so-called discontinuous growth bands (DG bands), has been reported for numerous polymers under certain test conditions [13]. It has been shown that these bands are representative of discrete crack advance increments following a period of many loading cycles of total crack arrest [13, 18–21]. Furthermore, some polymers have been found to exhibit shear lips reflecting fatigue crack propagation under plane stress conditions [22–24].

One feature, common to all of the above markings with the exception of arrest bands, is that their characteristic dimensions generally are proportional to some power of the stress intensity factor range, ΔK.

showed stress whitening in the stable crack growth regime, an indication of plastic deformation and extensive damage zone development. Some examples, which also reveal that the degree of whitening decreases abruptly at the transition to fast fracture, are shown in Fig. 3. On the other hand, comparatively little whitening was observed in the more brittle PS composites, and the transition point from stable fatigue crack advance to fast fracture was difficult to establish macroscopically.

A closer examination revealed some additional differences, at least for the materials of Series A. For
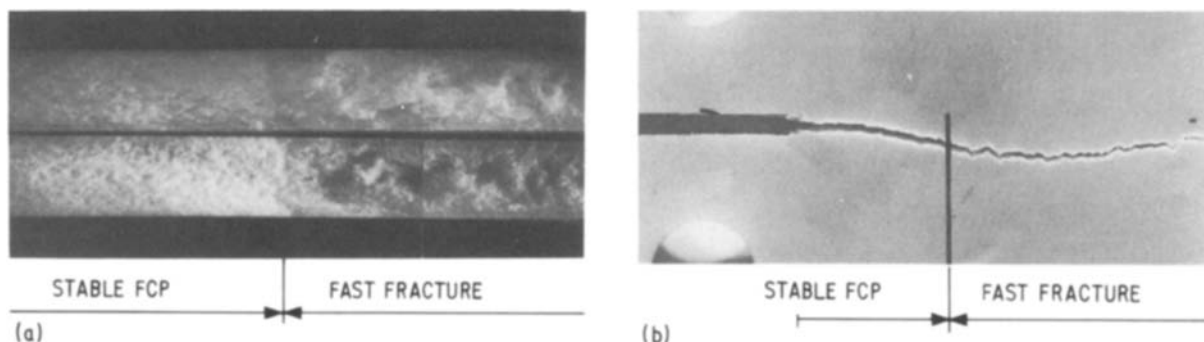

Figure 4 Transition region from stable FCP to fast fracture. (a) Fracture surface of N66-18G(A-T); and (b) side view of crack profile in N66-18G(A-L).
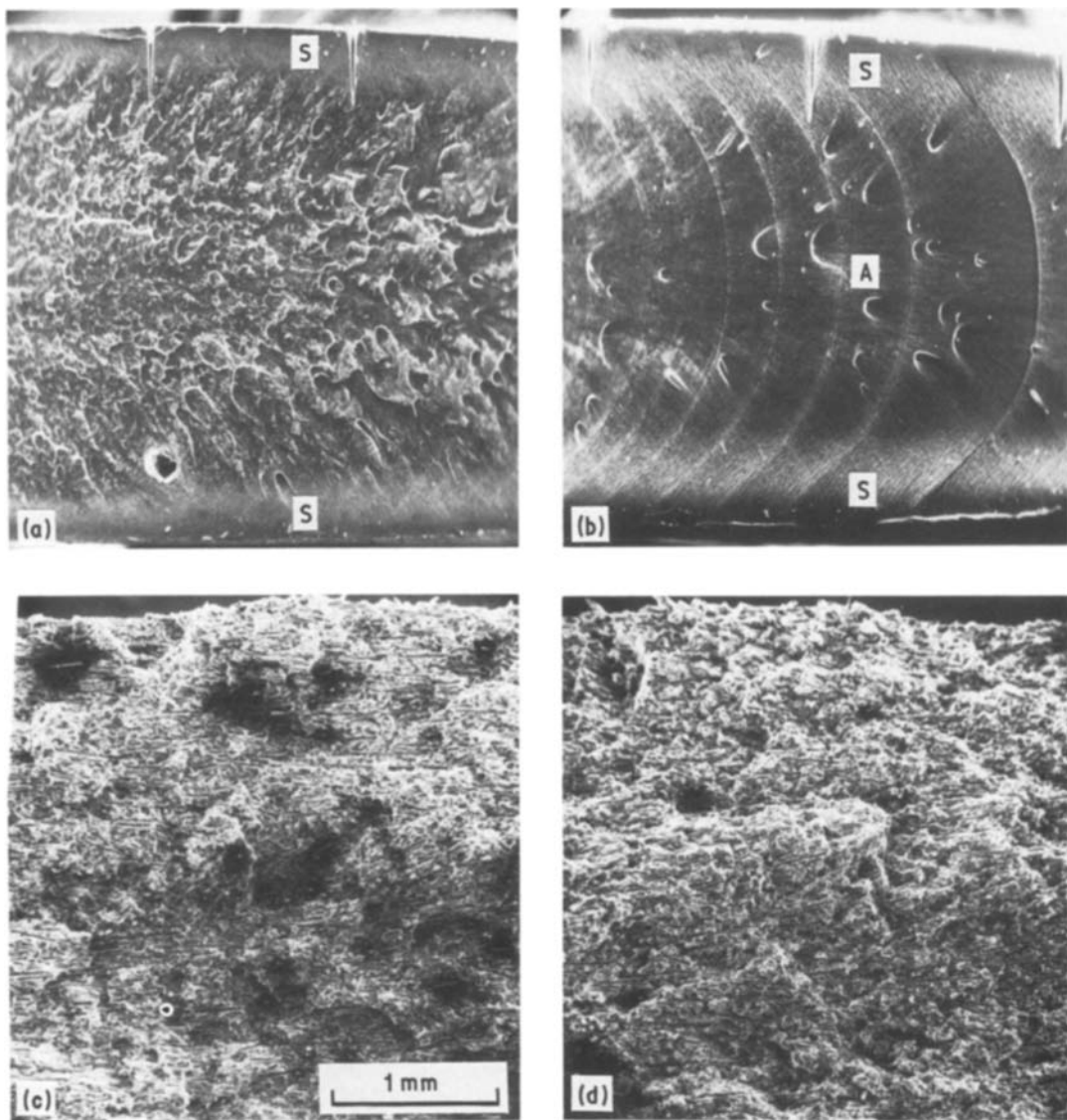
Figure 5 Low-magnification micrographs of stable FCP fracture surfaces in the nylon 66 systems of Series B. (a) Shear lips (S) in the neat matrix at low ΔK levels; (b) shear lips (S) and arrest bands (A) in the neat matrix at higher ΔK levels; (c) N66-16G(B-T); and (d) N66-31G(B-T).

Consequently, the establishment of precise relationships between the prevailing stress intensity conditions and any characteristic fracture surface detail from FCP experiments provides important quantitative information for applications in the field of failure analysis.

Typical low-magnification micrographs of FCP fracture surfaces of some unreinforced matrix materials are compared to their corresponding sgfr compositions in Figs 5 and 6. Some of the markings frequently observed in polymeric solids are clearly visible in the fractographs of the neat matrices. For example, a set of rather widely spaced arrest lines associated with the periodic interruptions of the FCP test to read the crack tip position is evident in Fig. 5b for N66 (Series B). Identical markings have been found previously by Bretz *et al.* [25] and related to the occurrence of creep. It should be mentioned, however, that these coarse arrest lines may also be at least, in part, due to transient effects related to crack tip cooling and hysteretic crack tip heating whenever cycling was interrupted and restarted. This possibility is not unreasonable considering the significant quasi-equilibrium temperature elevations of up to 35° C that

have been recorded at the crack tip under these test conditions [8].

In addition, evidence for the formation of shear lips whose fracture surfaces formed an angle with the flat regions in the centre of the specimen and whose dimensions increased with increasing ΔK was found in the case of N66 (Series B) [8, 24]. The shear lip regions are discernible at the free surfaces in Figs 5a and b by their distinctly different texture and their white appearance. Finally, discontinuous growth bands can be seen in the micrograph of the fracture surface of PS (Series B) in Fig. 6a. Again, the spacing between adjacent DG markings increases with increasing crack length and hence with increasing ΔK.

As mentioned above, an important aspect of the occurrence of any markings of this kind on fatigue-fracture surfaces is that they may be extremely valuable for quantitative interpretations with regard to the loading history and conditions experienced by a failed component. It is unfortunate, therefore, that no fractographic details of similar nature could be identified on the fracture surfaces of the composites investigated in this study. It should be mentioned, however,
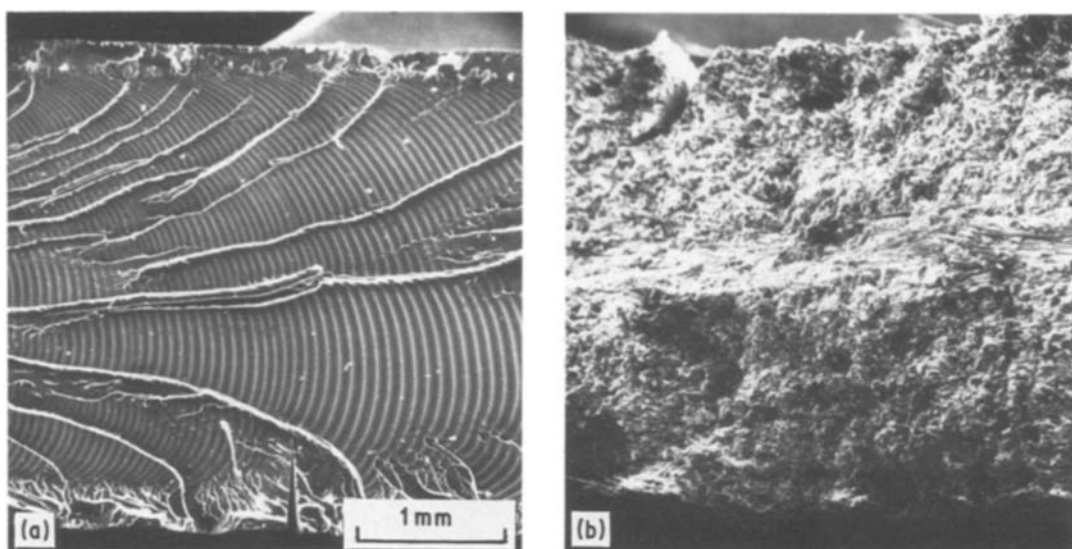
Figure 6 Low-magnification micrographs of stable FCP fracture surfaces in the poly(styrene) systems of Series B. (a) Discontinuous growth (DG) bands in the neat matrix; and (b) PS-18G(B-T).

that the existence of concentric lines in localized regions around individual fibres has been reported in quite a few cases [1, 2, 17, 26]. Although these markings provide some evidence for a fatigue failure mechanism, it is doubtful that such local fracture surface lineage could be used to establish reliable quantitative correlations with the overall applied loading conditions. Nevertheless, as will be shown in the following sections, valuable information on the micromechanisms of FCP in sf-composites can be obtained from a microscopic analysis of other fracture surface characteristics.

3.2.2. Characteristic fracture surface features

As has been shown previously for some sgfr composites [6, 9, 27], fracture surfaces generated by stable FCP reveal some features distinctly different from those produced by monotonic loading or fast fracture. Figs 7 and 8 represent fractographs of regions in N66-18G(A) and PS-18G(B), respectively, where

fibres are oriented at intermediate to high angles to the crack plane. Most strikingly, the length over which fibres are pulled out from the matrix is considerably higher in regions generated by monotonic or fast fracture, independent of matrix ductility and interfacial bond strength. However, the generally higher fibre pull-out length on monotonic or fast fracture surfaces of the PS composites in comparison to N66 (Series A) composites is one indication of the lower degree of adhesion in the former system. In addition, the overall appearance of both monotonic and fast fracture surfaces appears to be much cleaner. There is substantial evidence for the occurrence of single and multiple fibre fracture in the stable FCP regions with pieces of broken fibre ends and fragments of detached matrix particles spread over the fracture surfaces (Figs 7a and 8a).

Other pronounced variations in the fracture surface appearance were discovered in the well-bonded systems of N66(A) and N612(A). While fibres generally
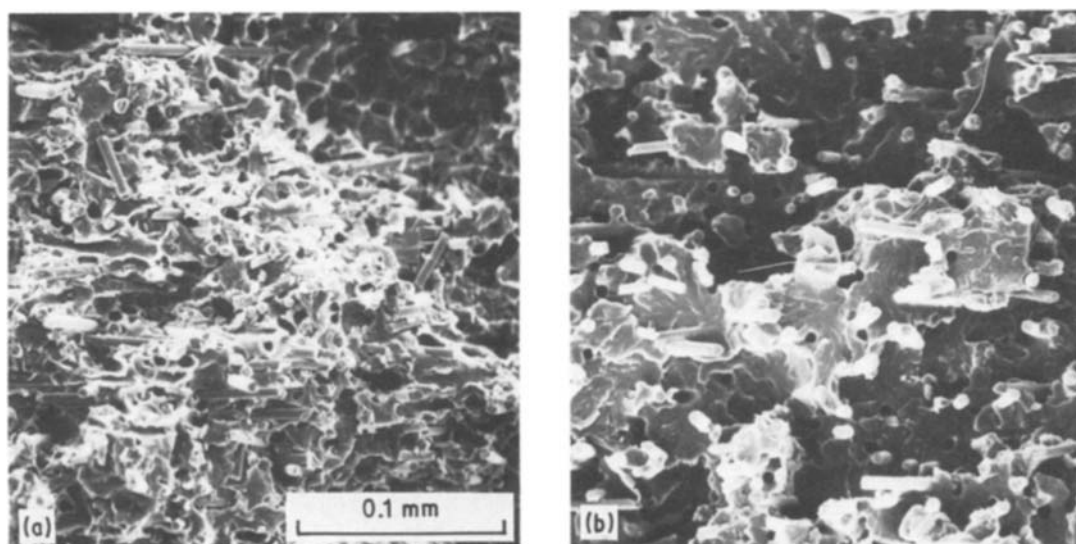

Figure 7 Comparison of fracture surfaces generated by different failure modes in the skin layer of N66-18G(A-L). (a) Stable FCP region; and (b) fast fracture region.
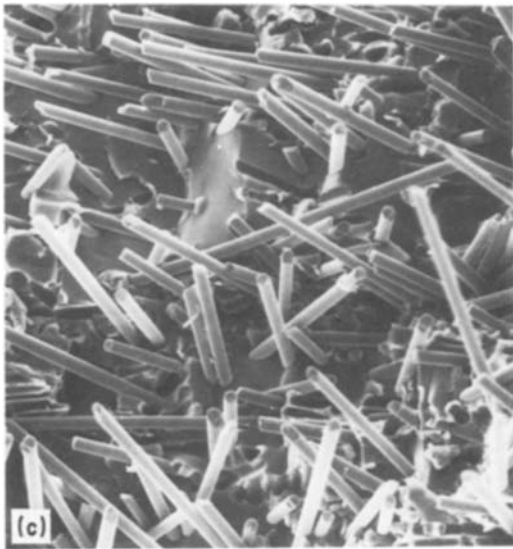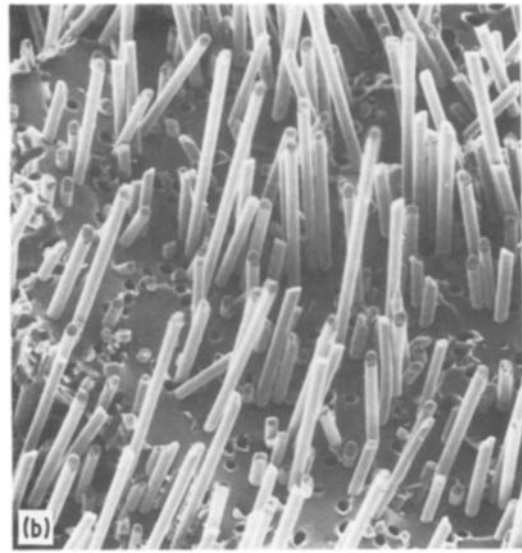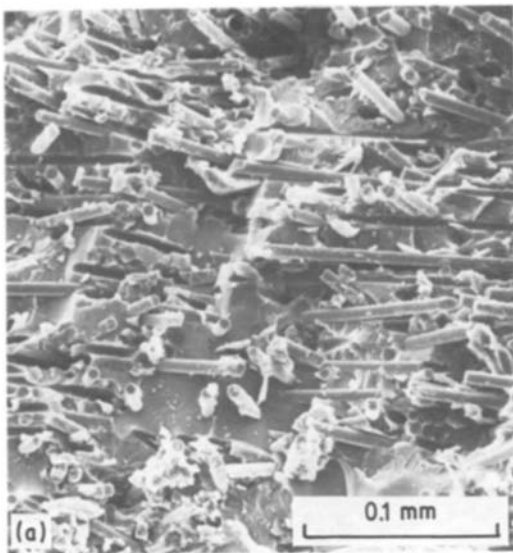
appeared to be clean and mirror-like in the stable FCP region, a high degree of interfacial adhesion was evident where fast fracture occurred. Characteristic micrographs illustrating these observations are shown side by side in Fi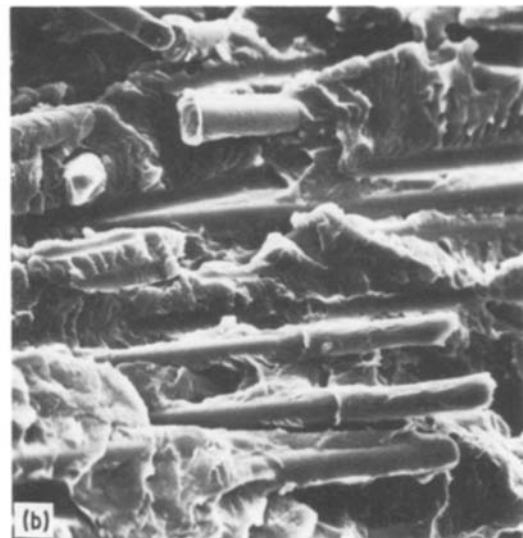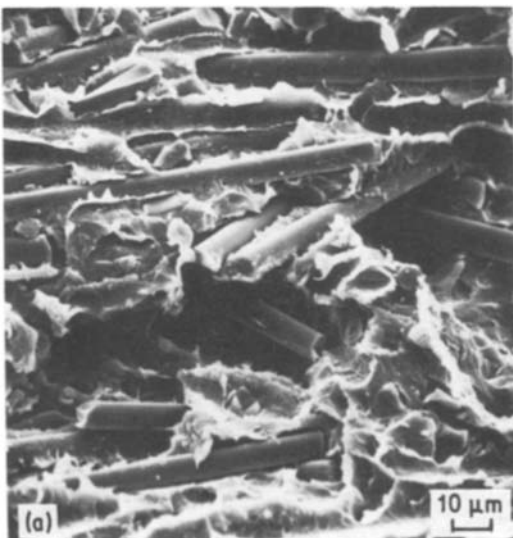gs 9 and 10 for fibres oriented mainly at small and large angles, respectively, to the main fracture plane. Furthermore, a higher degree of matrix drawing, indicative of ductile failure, was frequently observed in these systems under stable FCP conditions, especially in areas between fibres forming small angles with the fracture plane (Figs 9a and 11).

Contrary to the clear differences in the well-bonded nylon systems (Series A), it was not possible to establish any pronounced differences in the interfacial failure mode between FCP and monotonic or fast fractures in the poorly bonded PS and N66(B) systems. Also, in contrast to recent findings by Matsumoto [26] on unnotched specimens of sgfr poly(ether imide), no evidence could be found for fibre-splitting along the fibre axis in any of the systems investigated. While this indicates that some of the failure micromechanisms occurring in unnotched and prenotched specimens might be significantly different, the much higher fibre content used in this study could have played a role.

Figure 9 Differences in the interfacial failure mode and matrix ductility between (a) stable FCP and (b) fast fracture in the well-bonded system of N66-18G(A-L) with fibres at small angles to the crack plane (core layer).
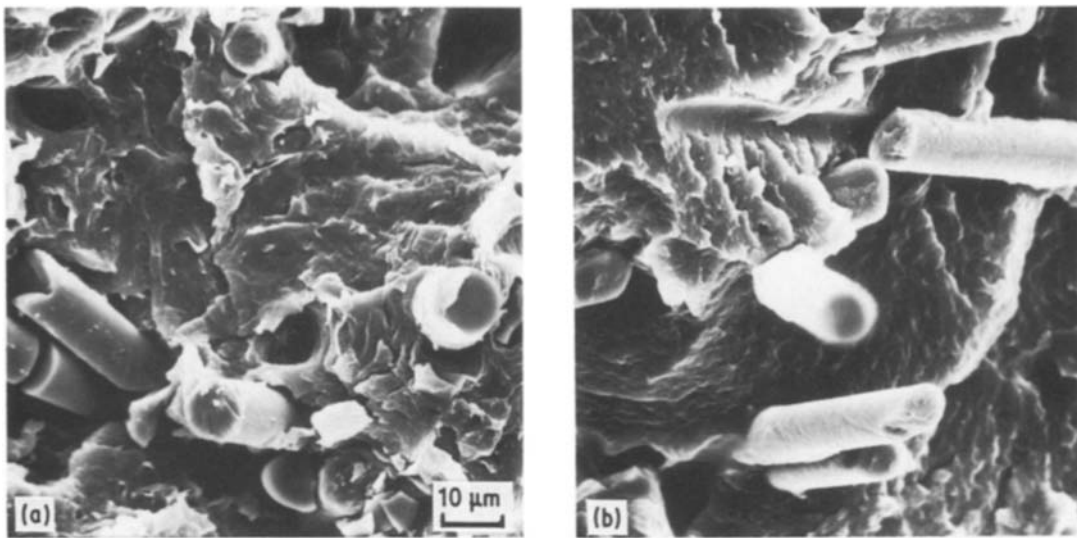
Figure 10 Differences in the interfacial failure mode and fibre pull-out length between (a) stable FCP and (b) fast fracture in the well-bonded system of N66-18G(A-T) with fibres at high angles to the crack plane (core layer).

3.3. Micromechanisms of failure

When a fatigue crack in sgfr plastics is grown intentionally from a notch, a complex damage zone develops at the crack tip. In general, fatigue cracks grow in a rather discontinuous way reflecting the changes in the local fibre agglomeration density and orientation just ahead of the crack tip. Similar to the case of crack growth under static or monotonic loading conditions [16, 17, 28, 29] the fatigue crack propagation process may involve many mechanisms such as fibre breakage, fibre debonding and pull-out, shear crack formation along fibres, plastic deformation and drawing of the matrix, void formation along with void coalescence, microcrack and craze development and coalescence, matrix fracture and crack branching. A typical example of crack branching also revealing some of the other local failure modes is illustrated in Fig. 12.

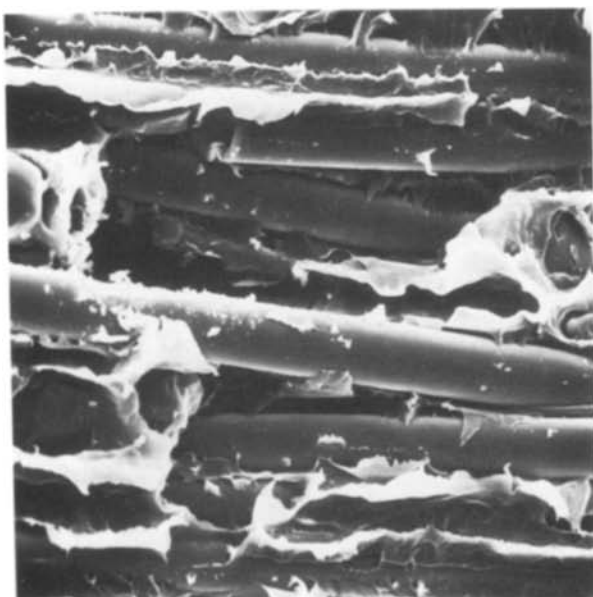The local modes of crack extension in sf-composites

depend on such microstructural parameters as local fibre orientation, matrix ductility and degree of interfacial adhesion. The large number of possible failure modes leads to a rather complex fracture surface appearance which makes it difficult to establish generally valid rules for the micromechanisms of failure. Nevertheless, based on the presented fractographic evidence, the following model is proposed for crack propagation under fast fracture and fatigue loading conditions.

3.3.1. Fibres at small angles to the crack plane

The most significant differences in the failure modes between stable FCP and fast fracture for local fibre orientations close to the crack plane and perpendicular to the applied load were illustrated in Figs 9 and 11 for the well-bonded systems of N66 and N612 of Series A. The difference in the interfacial failure site between fast fracture (matrix-covered fibres in Fig. 9b)
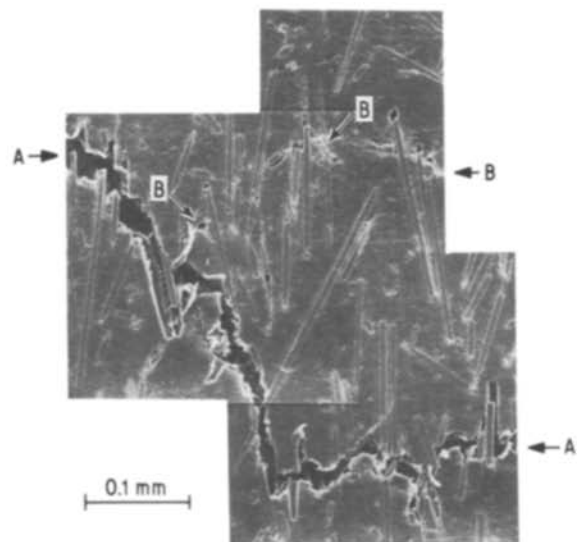

Figure 11 High degree of matrix ductility in the stable FCP region of N612-25G(A-T) with fibres at small angles to the crack plane (skin layer); fibre diameter $\approx 10\,\mu m$.

Figure 12 Side view of a fatigue cracked region in N66-18G(A-L) showing the main crack (A) as well as a secondary crack (B) branching off the main crack.
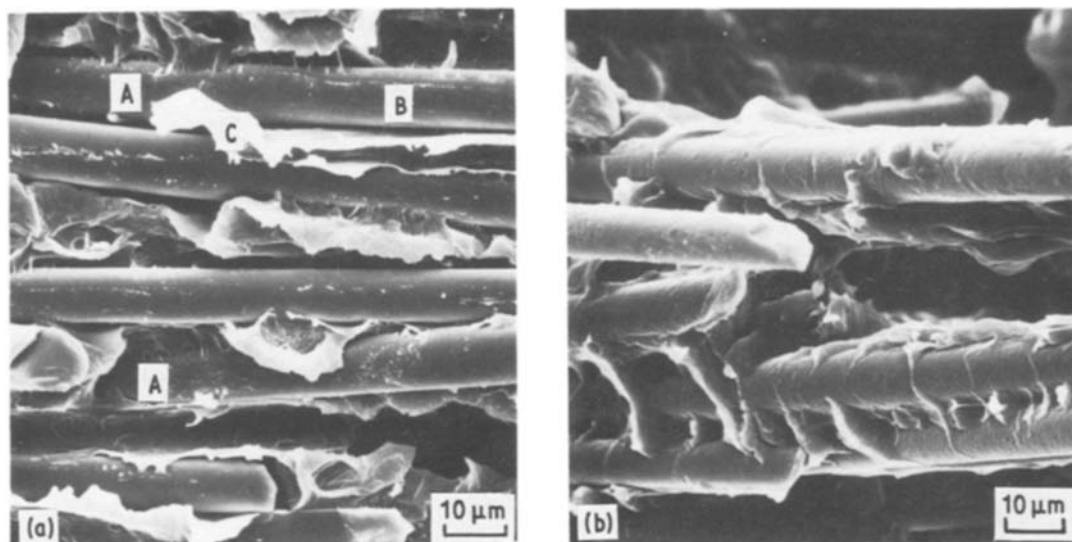
Figure 13 Fractographs revealing some of the micromechanisms of crack advance in the well-bonded system of N66-18G(A-T) in regions with fibres at small angles to the crack plane. (a) Stable FCP region: microvoid formation (A), extensive debonding along fibre (B), and matrix drawing (C); and (b) fast fracture region.

and stable FCP (mirror-clean fibres in Figs 9a and 11) suggests, of course, that fatigue loading has a more damaging effect on the interface than on the polymeric matrix. With the help of some higher magnification micrographs the following sequence of events is suggested to have developed the distinctly different morphologies (Fig. 13).

Cyclic damage ahead of a pre-existing crack starts as highly localized debonding from statistically distributed micro-regions of poor adhesion that invariably exist along the fibre/matrix interface even in well-bonded materials. The localized separation of the matrix from the fibres leads to the formation of microvoids reminiscent of those involved in craze formation in unreinforced polymers (Regions A, Fig. 13a). Continued fatigue loading results in the growth of these microvoids by further debonding along the interface and leads to microvoid coalescence so that the matrix eventually detaches from the fibres over larger areas (Region B, Fig. 13a). If extensive local debonding occurs prior to matrix separation by the propagating crack, the matrix is able to pull away from the adjacent fibres, thereby leading to a local reduction of the stress component perpendicular to the direction of fibre orientation. Under these circumstances the matrix may deform (presumably in a shear deformation mode) and then ultimately fail under plane stress conditions. The increased deformability associated with the plane stress deformation mode is evident in the extensively stretched matrix segments between fibres (Region C, Fig. 13a; see also Figs 9a and 11).

This failure mode for stable FCP in the well-bonded systems is clearly different from the fast fracture mode. Fibres on fracture surfaces generated by the latter conditions are still covered with a thin layer of material, and matrix failure itself appears to be more brittle (Figs 9b and 13b). Apparently, the micro-regions of poor adhesion at the fibre/matrix interface are not sufficiently weakened under the application of rapid monotonic loads to allow for extensive inter-

facial microvoid development and growth prior to material separation by the advancing crack. Thus failure in this case occurs close to, although not quite at, the interface by tensile or shear failure of the matrix.

While it is difficult to quantitatively estimate to what extent the coupling agent and the polymeric matrix, respectively, are involved in the composition of the interfacial layer on fast fracture surfaces, the difference in the local failure site may help to explain the apparent change in the matrix failure mode. For example, it is conceivable that the high degree of adhesion exhibited under fast fracture conditions increases the constraint on the matrix by introducing a local stress component perpendicular to the fibres. This enhances the severity of the local stress field and reduces the matrix deformability and the tendency for matrix drawing. In addition, the higher local strain rates associated with the higher crack speeds under fast fracture conditions undoubtedly contribute to the increased tendency for brittle matrix failure.

As mentioned above, no significant changes in the interfacial failure mode between monotonic and cyclic failure could be observed in the poorly bonded compositions of PS and N66 (Series B) not even at high magnifications (Fig. 14). This is not surprising, however, because it can be expected that the least crack resistant path under these circumstances should be the one along the weak fibre/matrix interface in either case.

A close inspection of the PS matrix failure adjacent to the fibres provides some information as to the local failure mode in this microstructural element. Although the higher magnification micrographs of such matrix fracture surfaces reveal some differences in the fine structure for PS composites fractured by stable FCP and by monotonic loading (Figs 15a and b), the overall appearances are reminiscent of those created by the discontinuous craze-breakdown mechanism in the unreinforced material (Fig. 16). Indeed the stretched
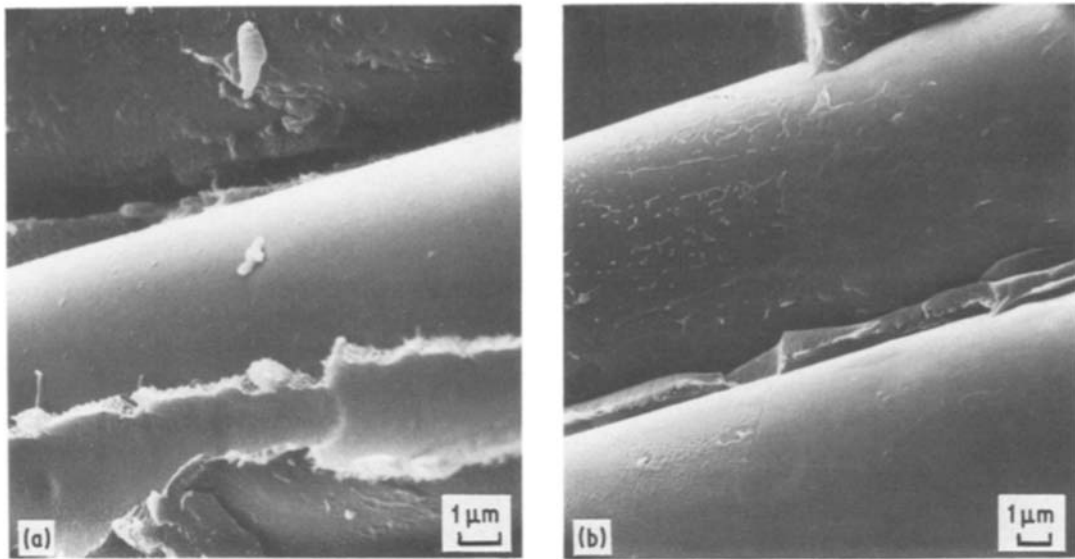
Figure 14 Interfacial failure in the poorly bonded system of PS-18G(B-T) at high magnification. (a) Stable FCP region; and (b) fast fracture region.

segments visible in the micrographs of Figs 15 and 16 closely resemble the remnants of craze fibrils similar to those observed by others [30, 31]. The variations in the fine structure and the associated smaller fibril length in Fig. 15b as compared to Fig. 15a may perhaps reflect the differences in the local crack speed and its effect on the craze formation and craze breakdown process. Hence it appears that matrix fracture in the PS composites may involve a similar or comparable craze-controlled process to the one in the unreinforced matrix itself. However, DG bands, as observed in the pure matrix and elsewhere for sgfr poly(ether imide) [26] could not be identified in the composites studied here, probably again as a result of the higher fibre content used. In addition, it should be recognized that depending on the local stress field between fibres and the preceding and surrounding local fractures within the crack-tip damage zone, matrix shear failure may also be important. Thus it is possible that the dark and relatively smooth area emanating from the lower left

corner in Fig. 15a has been created by the latter fracture mechanism.

3.3.2. Fibres at large angles to the crack plane

The main question regarding the differences between stable FCP and fast fracture in regions where fibres are at large angles to the crack plane is related to the higher degree of fibre fracture under FCP conditions. While it is well-known that cyclic loading reduces the strength in almost all materials, a fatigue failure of fibres in a pure tensile mode as the dominant mechanism appears unlikely for the following reasons. Because fibre pull-out was found to be the dominant mechanism during fast fracture and monotonic loading conditions (Figs 7b, 8b and c), fibre tensile failure in fatigue would imply a more degrading effect of cyclic loading on the fibre tensile strength than on the interfacial shear strength. This is inconsistent, however, with (1) the comparatively mirror-like appearance of
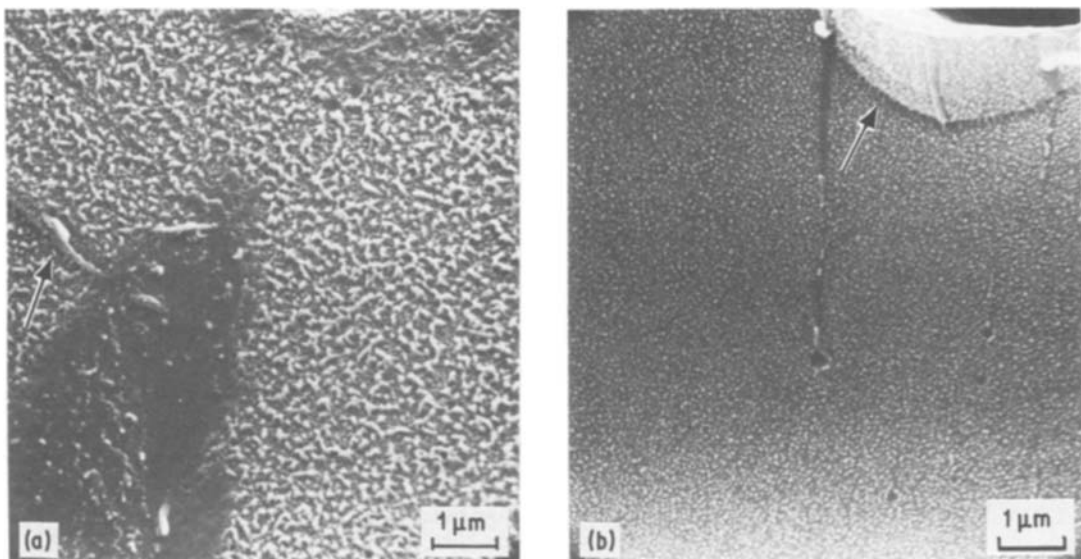

Figure 15 Fracture surface morphology of matrix failure between fibres in PS-18G(B-T) indicative of a craze formation and craze breakdown process. (a) Stable FCP region; and (b) fast fracture region. Note secondary crazes indicated by arrows.
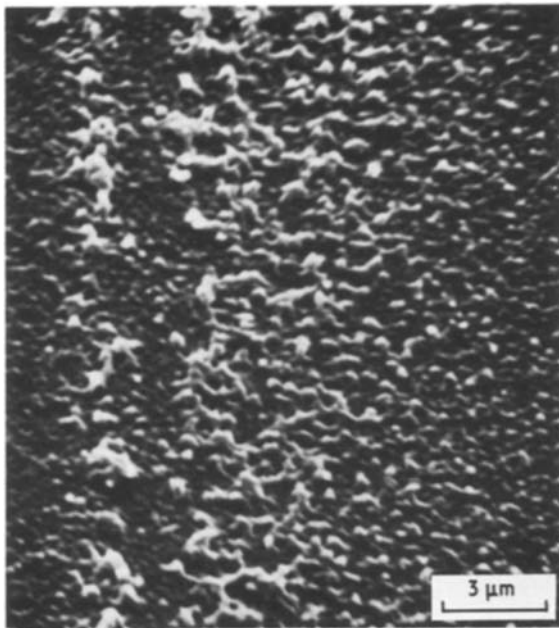
4024

Figure 16 Micromorphology of discontinuous growth band in unreinforced PS(B).

fibres on the FCP fracture surfaces of the well-bonded materials of Series A (Fig. 10a) and (2) with the rather low interfacial shear strength of the poorly bonded materials of Series B to begin with. Therefore the following model is proposed for fatigue crack advance under these conditions.

When a fatigue crack in a short fibre composite grows into a region where fibres are oriented at high angles to the crack plane, damage initiation ahead of the main crack may occur in several ways. Because of the stress concentration associated with the presence of fibre ends [28] and consistent with recent observations under monotonic loads [29, 32, 33] it seems reasonable to assume that the fibre ends become the first sites for damage initiation (i.e. plastic deformation of the matrix, and microcrack and craze formation) and debonding (Fig. 17a). This can be

expected especially for fibres whose ends are close to the main crack plane. Crack extension under these circumstances may then simply occur by growth and coalescence of these micro-damage zones with each other and the main crack. In cases where a fatigue crack approaches fibres whose ends are sufficiently far away from the main crack plane and therefore in a lower stress region, debonding may occur first somewhere along the fibre ahead of the crack tip. Such initial, localized debonding at sites other than at fibre ends (and in some instances even fibre fracture) may also take place because of stress concentration effects associated with adjacent fibres (Fig. 17b).

In any case, independent of where local debonding occurs first, continued cycling will tend to propagate micro-shear cracks along the interface. The clean fibre appearance of the FCP fracture surfaces even in the well-bonded systems (Fig. 10a) suggests that such micro-shear crack formation and growth takes place directly at the interface rather than in the adjacent matrix as observed in fast fracture (Fig. 10b). In fact from the appearance of the fibre bed surface in Fig. 17b one may conclude that the precursors of such interfacial shear cracks are again microvoids as was the case for fibres at small angles to the crack plane which, however, now form and coalesce under shear stress conditions.

At some point when the interface is sufficiently weakened, a fibre is being pulled out at least over part of its length with the main crack or a secondary crack eventually by-passing the fibre (Fig. 17a). Such unbroken fibres may still have some load-bearing capability due to load transfer by frictional forces. Hence, compressive stresses develop in individual fibres in subsequent unloading cycles due to both the frictional resistance associated with fibre sliding, and the overall compressive stresses acting upon the crack tip damage zone (this concept is analogous to that which causes reversed plasticity in homogeneous materials [12]). In addition, cyclic fibre bending associated either with mechanical interlocking if the
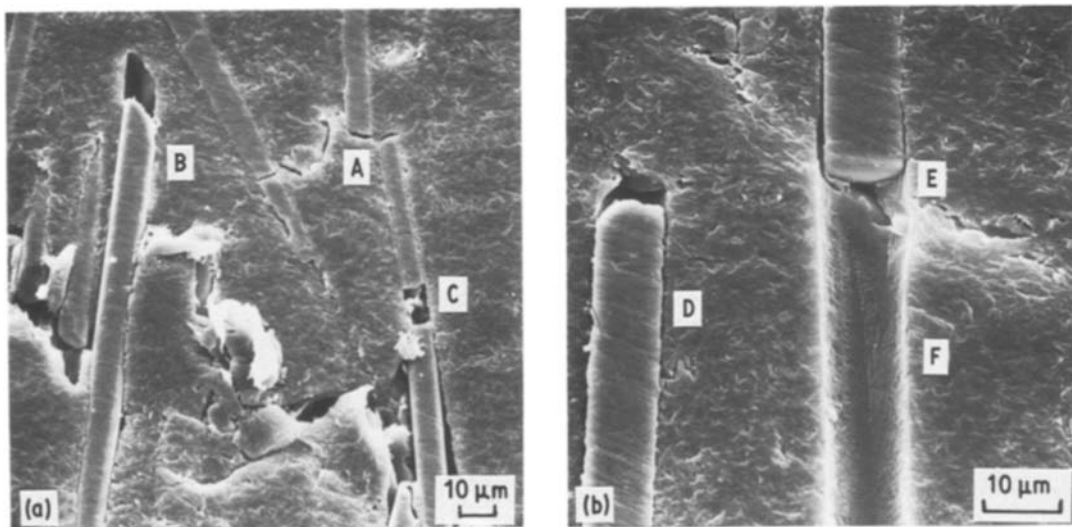

Figure 17 Fatigue crack propagation in N66-18G(A-L) viewed on the side surface in regions where fibres are at high angles to the nominal crack plane. (a) Debonding at fibre ends (A), fibre pull-out (B) fibre failure (C); and (b) shear crack formation along fibre interface (D), fibre fracture due to stress concentration associated with adjacent sub-surface fibre (E), and fibre bed revealing evidence for a microvoid coalescence mechanism (F).
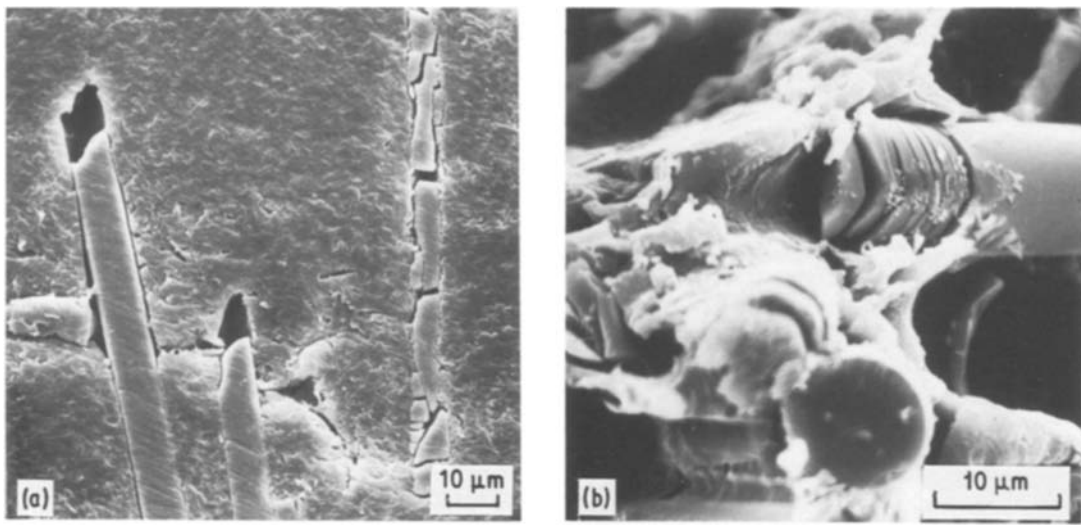
Figure 18 Multiple fibre failure in N66-18G(A-L) associated with the development of significant local compressive stresses during unloading despite an overall applied tensile/tensile mode of fatigue loading. (a) Side surface view in stable FCP region; and (b) fracture surface in stable FCP region.

crack does not open exactly along the fibre axis, or as a result of rotational displacements within the crack tip damage zone, are probably important. The development of significant compressive or flexural stresses along with the comparatively low resistance of glass fibres to these deformation modes (in part due to the high tendency towards elastic instability in compression) causes fibres ultimately to break in compression or flexure, or by microbuckling. Examples lending strong support to such failure modes are shown in Fig. 18 for N66-18G(A). Although it should be mentioned that such remarkable examples of multiple fibre fracture are not frequently observed (partly because broken fibre fragments may not always remain on the fracture surface), they do highlight and support the hypothesis of compressive and flexural fibre failure [9, 27]. A tensile failure mechanism causing such effects is indeed difficult to conceive.

3.3.3. Fibres at intermediate angles to the crack plane

Because of the already mentioned detrimental effect of

fatigue loading on the interfacial strength, we may here also expect damage initiation and propagation in the form of micro-shear cracks along and around fibres at the interface (Fig. 19a). As with the previous case, a crack may again by-pass fibres, especially if they are agglomerated in fibre bundles, an effect which contributes to the macroscopic zig-zag appearance of the crack path. In the case of shear-crack formation at and around more isolated fibres, which may also lead to subsequent partial fibre pull-out, stresses can still be transferred even in the wake of the advancing crack either by interfacial friction or incomplete debonding, or simply by mechanical interlocking associated with inclined fibres bridging the crack. As a result of the cyclic changes in the applied load, cyclic bending stresses develop in these fibres which ultimately may cause fibre failure under flexure (Fig. 19b). In contrast to the failure mode for fibres at high angles to the crack plane described above, fibres may now fail during the loading or the unloading part of a fatigue cycle.
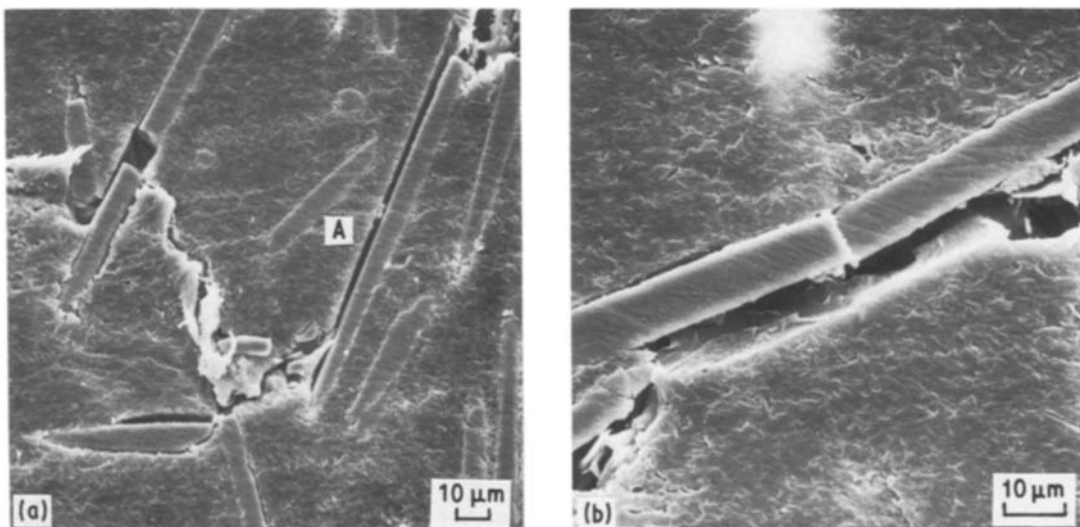

Figure 19 Fatigue crack propagation in N66-18G(A-L) viewed on the side surface in regions where fibres are at intermediate angles to the nominal crack plane. (a) Shear crack growth around fibre (A); and (b) fibre failure in a bending mode.
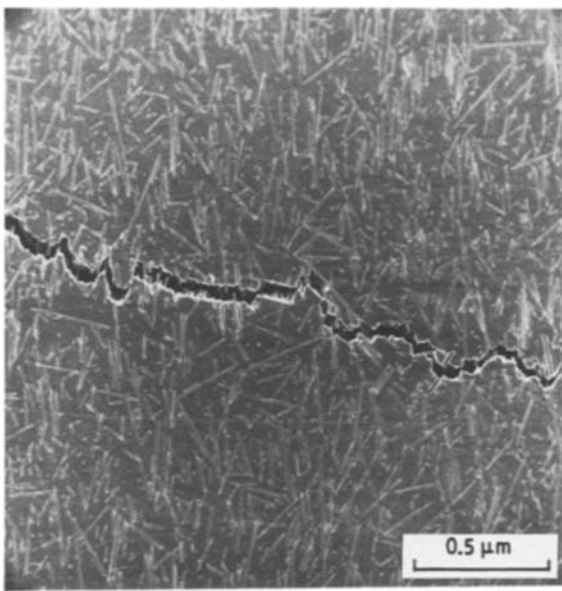
Figure 20 Low-magnification micrograph of a section of the crack trajectory on a polished surface in N66-18G(A-L).

3.3.4. Crack closure effects

Another important aspect in sfr plastics subjected to cyclic loads is related to crack closure. Several crack closure mechanisms have been used in FCP studies of metallic materials to explain effects related to over-loads, variations in load ratio, environmental effects, and near threshold crack growth behaviour [12, 34–40]. A common feature to all these mechanisms is the assumption that the crack surfaces interfere in the wake of the advancing crack front and cause the crack to close partially above the minimum applied tensile load level. One of the proposed mechanisms, termed roughness-induced crack closure [38], has been applied most recently to the case of sfr plastics [41]. The contribution of a roughness component to crack closure is thought to be important when the magnitude of the fracture roughness is comparable to the crack tip opening displacement, and in cases where Mode II (in-plane shear) displacements exist [37–39].

An overall view of the crack profile in N66/18G(A–L) is depicted in Fig. 20. Clearly, the local variations in the crack path associated with the zig-zag crack propagation mode, as well as the tendency of some materials to produce cracks that do not always propagate perpendicular to the applied loads (i.e. non-coplanar crack growth or crack curvature, Fig. 2) in effect introduce a Mode II contribution in the crack tip displacements.

The mechanisms causing roughness-induced crack closure in short-fibre composites are depicted schematically in Fig. 21. First, consider the overall or macro-roughness of the serrated fracture surface profile (Figs 4 and 20). As illustrated in Fig. 21a, the perfect mating of the fracture surfaces is lost as a result of the combination of Mode I/Mode II displacements. The horizontal displacement between the crack faces associated with the in-plane shear deformation mode (Mode II) leads to crack surface contact over discrete regions on unloading [37–39]. Crack surface interference in sf-composites is further promoted by the formation of facets that assume the shape of
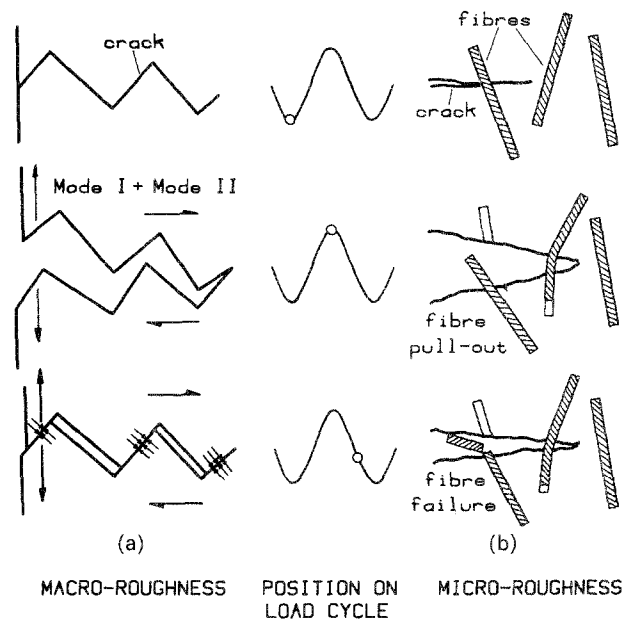

Figure 21 Sequence of mechanisms associated with roughness-induced crack closure in short–fibre composites. (a) Crack closure at discrete contact areas due to the local Mode II contribution in the displacements associated with the overall crack surface roughness as suggested in [37, 38]; and (b) crack surface interference on a microscale as a consequence of fibre pull-out.

undercuts and hence cause mechanical interlocking between roughness elements of opposite fracture surfaces. Such interlocking is, of course, beneficial to the FCP resistance, because part of the externally applied crack driving force is being dissipated in lifting interlocked asperities past each other.

A second mechanism, one which considers fracture surface roughness on a more localized scale (micro-roughness) is related to the occurrence of fibre pull-out. Fig. 21b illustrates schematically how a fibre, after being by-passed by the propagating crack is first pulled out during loading and subsequently is broken (either in compression, bending or by buckling) between the closing crack faces during unloading.

The fact that the crack surfaces in FCP experiments even under tensile/tensile conditions interfere on unloading before the applied load reaches its minimum has led to the suggestion that many of the characteristics unique to stable FCP fracture surfaces in sf-composites (e.g. higher degree of single and multiple fibre fracture, Figs 7 and 8) are, in part, due to compressive forces acting in local regions along the crack flanks, and the friction and wear associated with repetitive fracture surface impingement [9, 41]. Further examples revealing some closure-related features such as the fracture surface debris in the form of detached matrix particles or the fine wear dust are shown in Fig. 22 for the semi-brittle and brittle systems, respectively, of N66 (Series A) and PS (Series B).

Of course, the tendency to generate these abrasion and wear products during repetitive crack face interference should also depend on the wear properties of the matrix as well as on the fibre orientation. For example, there was significantly less evidence for some of these features in the composites of the more ductile systems of N66 (Series B)(Fig. 23). In addition, because crack surfaces are generally more planar in
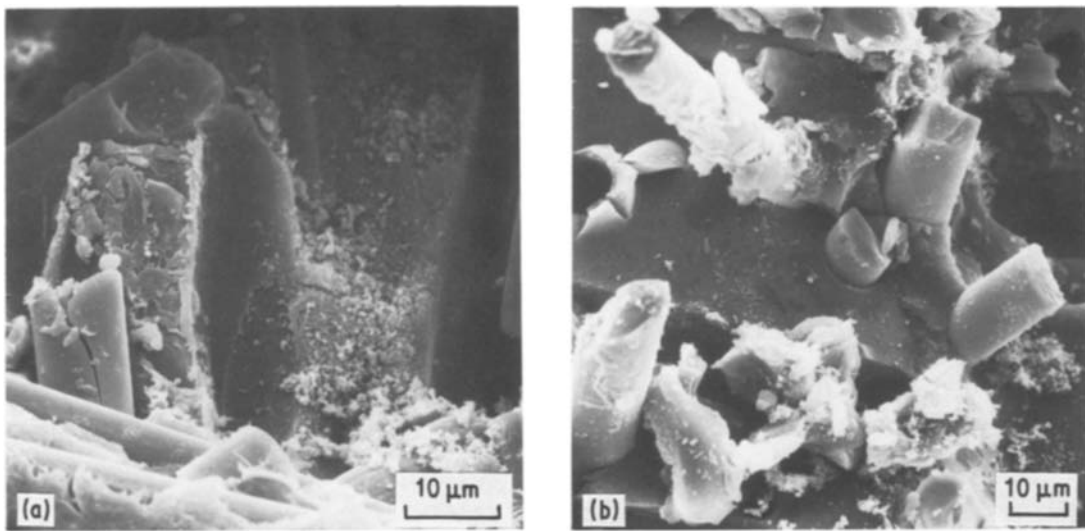
4027

Figure 22 Micrographs from the stable FCP region showing fracture surface debris generated by pronounced crack face interference and fibre sliding. (a) N66-18G(A-L); and (b) PS-18G(B-T).

regions where fibres are at small angles to the crack plane, it follows that crack closure related features should be less pronounced in such areas. Indeed, some of the characteristics shown in Fig. 22 are clearly less apparent on the fracture surfaces shown in Fig. 24 and in Figs 9a, 11 and 13a.

3.3.5. Implications

Several implications of the micromechanisms associated with fatigue crack advance in sf-composites are worth mentioning. One consequence of the roughness-induced crack closure concept is that a higher degree of fracture surface roughness may promote crack closure effects according to the previous discussion. Thus the more serrated fracture surface in regions where fibres are at high angles to the crack plane may result in crack closure loads and, therefore, in crack closure stress intensities, K_{cl} (stress intensity level at which crack closure occurs on unloading) that are higher than those for regions where fibres are oriented

more nearly parallel to the overall crack plane. Assuming a constant maximum stress intensity level, K_{max}, this implies a lower value for the effective stress intensity factor range, ΔK_{eff} ($\Delta K_{eff} = K_{max} - K_{cl}$) for the former fibre orientation. Analogous to the mechanism suggested to explain grain size effects on the FCP resistance of metals in the threshold regime [37–40], such a decrease in ΔK_{eff} should be beneficial and may perhaps contribute to the higher FCP resistance observed for specimens with fibres oriented predominantly at high angles to the anticipated crack plane [3, 7, 9]. There are, of course, other factors such as the increased load-bearing capability of the fibres, the higher stiffness, and the more energy consuming path of the crack that cause the improved FCP resistance in the latter case.

Two more implications follow from the fact that fibre failure during stable FCP is attributed primarily to deformation modes such as compression, flexure and buckling. First, the occurrence of massive fibre
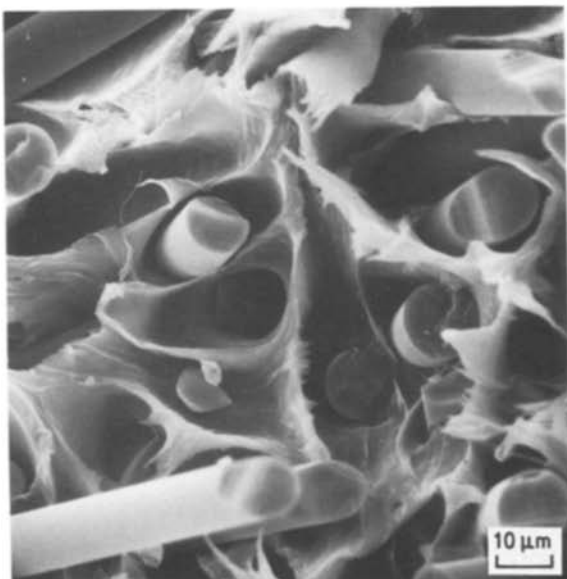
Figure 23 Stable FCP fracture surface in the ductile system of N66-16G(B-T) with fibres at high angles to the crack plane.
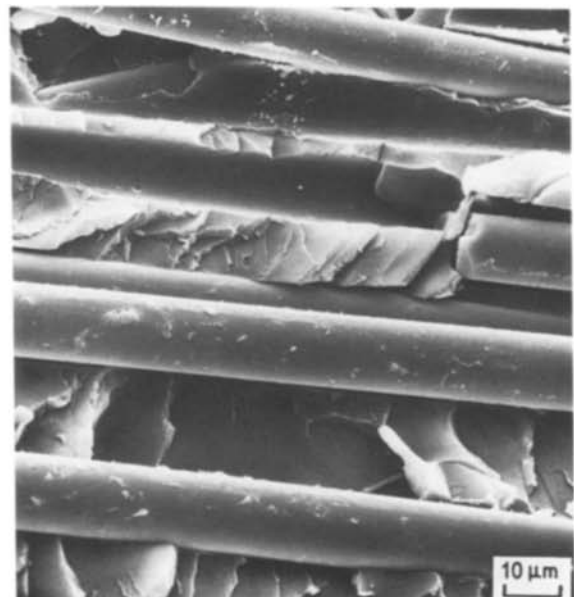
Figure 24 Stable FCP fracture surface in the brittle system of PS-18G(B-T) with fibres at small angles to the crack plane.
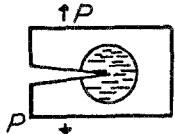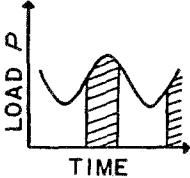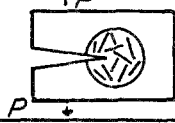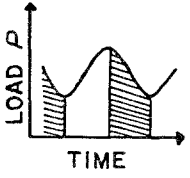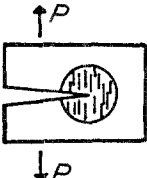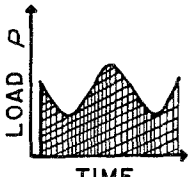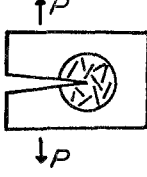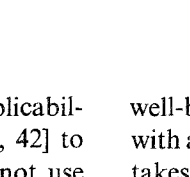
LOCAL' FIBRE ORIENTATION	MAIN FAILURE MODES	LOADING CYCLE
↑P P↓	TENSILE OR SHEAR FAILURE IN THE MATRIX AND AT THE INTERFACE	LOAD P / TIME
↑P P↓	SHEAR FAILURE AT THE INTERFACE	LOAD P / TIME
↑P ↓P	SINGLE AND MULTIPLE FIBRE FRACTURE IN COMPRESSION, BY BUCKLING OR DURING CRACK CLOSURE	LOAD P / TIME
↑P ↓P	FIBRE FRACTURE IN A BENDING MODE OR DURING CRACK CLOSURE	LOAD P / TIME

Figure 25 Summary of the most important micro-modes of failure during stable FCP in sgfr plastics.

failure by these mechanisms eliminates the applicability of the classic "shear lag" analysis [15, 28, 42] to FCP fracture surfaces and therefore one cannot use the apparent fibre pull-out length to estimate the interfacial shear strength during stable FCP. Second, fibre failure in compression, bending or by buckling indicates that an improvement in the fibre tensile strength may not necessarily improve the FCP resistance of these materials. From the standpoint of FCP it appears desirable to use and to develop fibres that are less prone to the failure modes mentioned above.

4. Summary and conclusions

Based on the fractographic evidence presented in this paper, several observations and conclusions about crack propagation mechanisms in short glass fibre-reinforced plastics may be noted:

1. Fracture surfaces in sgfr plastics generated by stable fatigue crack propagation reveal several distinctly different features from those produced by unstable fracture or by crack growth under monotonic loads. Among the most striking differences are the generally higher degree of single and multiple fibre fracture during FCP, and the differences in the interfacial failure site in well-bonded systems.

2. For good interfacial adhesion, crack advance along fibres under stable FCP conditions occurs by the formation and coalescence of microvoids and microcracks directly at the interface because of the adverse effect of fatigue loading on the interfacial bond strength. By contrast, in the fast fracture region of the well-bonded systems fibres were found to be covered with a thin interfacial layer which indicates that failure takes place in the adjacent matrix.

3. In the case of poor interfacial adhesion crack advance under both stable fatigue and fast fracture conditions occurs, of course, directly at the interface.

4. Some important failure events during stable FCP are summarized and related to where they occur on the loading cycle in Fig. 25. Tensile or shear failure associated with crack advance through the polymeric matrix or along the fibre/matrix interface is believed to take place predominantly in the upper portion of a fatigue cycle. In sharp contrast, fibre fracture occurs primarily during the unloading part of a fatigue cycle, either as a result of compressive stresses which develop within the crack tip damage zone, or because of fracture surface interference in the wake of the advancing crack front (roughness-induced crack closure).

5. No fractographic features could be identified in any of the sfr materials investigated that would allow the establishment of reliable, quantitative relationships between characteristic fracture surface details and the prevailing test or loading conditions or the rate of crack advance.

Acknowledgements

References

1. A. T. DiBENEDETTO, G. SALEE and R. HLAVACEK, *Polym. Engng. Sci.* **15** (1975) 242.
2. J. F. MANDELL, D. D. HUANG and F. J. McGARRY, *Polym. Compos.* **2** (1981) 137.
3. R. W. LANG, J. A. MANSON and R. W. HERTZBERG, in "Multiphase Polymer Systems–Polymer Blends and Composites", edited by C. D. Han, Advances in Chemistry Series No. 206 (American Chemical Society, Washington, D.C. 1984) p. 261.
4. M. SUZUKI, M. SHIMIZU, E. JINEN, M. MAEDA and M. NAKAMURA, Proceedings of the International Conference on Mechanical Behaviour of Materials, Vol. 5 (Kyoto, 1971) p. 279.
5. A. T. DiBENEDETTO and G. SALEE, *Polym. Engng. Sci.* **19** (1979) 512.
6. R. W. LANG, J. A. MANSON and R. W. HERTZBERG, *ibid.* **22** (1982) 982.
7. K. FRIEDRICH, *Kunststoffe* **72/5** (1982) 290.
8. R. W. LANG, J. A. MANSON and R. W. HERTZBERG, in "The Role of the Polymeric Matrix in the Processing and Structural Properties of Composite Materials", edited by L. Nicholais and J. C. Seferis (Plenum, New York 1983) p. 377.
9. R. W. LANG, J. A. MANSON and R. W. HERTZBERG, *ACS Organic Coatings and Plast. Chem.* **48** (1983) 816.
10. J. F. MANDELL, F. J. McGARRY, D. D. HUANG and C. G. LI, *Polym. Compos.* **4** (1983) 32.
11. G. M. CONNELLY, C. M. RIMNAC, T. M. WRIGHT, R. W. HERTZBERG and J. A. MANSON, Transactions of the 30th Annual Orthopaedic Research Society Meeting, Vol. 9 (1984), p. 293.
12. R. W. HERTZBERG, "Deformation and Fracture Mechanics of Engineering Materials", 2nd Edn. (Wiley, New York, 1983).
13. R. W. HERTZBERG and J. A. MANSON, "Fatigue of Engineering Plastics" (Academic, New York, 1980).
14. G. MENGES and P. GEISBUSCH, *Colloid Polym. Sci.* **260** (1982) 73.
15. M. J. FOLKES, "Short Fibre Reinforced Thermoplastics" (Research Studies Press, Chichester, 1982).
16. J. F. MANDELL, A. Y. DARWISH and F. J. McGARRY, ASTM STP 734 (American Society for Testing and Materials, Philadelphia, Pennsylvania, 1981) p. 73.
17. K. FRIEDRICH, Fortschr.-Ber. VDI-Z., Reihe 8, Nr. 12 (VDI-Verlag GmbH, Dusseldorf, 1982). (German report).
18. J. P. ELINCK, J. C. BAUWENS and G. HOMÈS, *Int. J. Fract. Mech.* **7** (1971) 227.
19. T. KUROBE and H. WAKASHIMA, *J. Soc. Mater. Sci.* **21** (1972) 800.
20. R. W. HERTZBERG and J. A. MANSON, *J. Mater. Sci.* **8** (1973) 1554.
21. L. KÖNCZÖL, M. G. SCHINKER and W. DÖLL, Proceedings of the International Conference on Fatigue in Polymers, Paper 4 (The Plastics and Rubber Institute, London, 1983).
22. J. A. MANSON and R. W. HERTZBERG, *CRC Crit. Rev. Macrom. Sci.* **1** (1973) 433.
23. G. PITMAN and I. M. WARD, *J. Mater. Sci.* **15** (1980) 635.
24. R. W. LANG, PhD dissertation, Lehigh University (1984).
25. P. E. BRETZ, R. W. HERTZBERG and J. A. MANSON, *J. Mater. Sci.* **16** (1981) 2070.
26. D. S. MATSUMOTO, *J. Mater. Sci. Lett.* **2** (1983) 7.
27. C. LHYMN and J. M. SCHULTZ, *J. Mat. Sci.* **18** (1983) 2029.
28. B. D. AGARWAL and L. J. BROUTMAN, "Analysis and Performance of Fiber Composites" (Wiley, New York, 1980).
29. J. F. MANDELL, D. D. HUANG and F. J. McGARRY, ASTM STP 772 (American Society for Testing and Materials, Philadelphia, Pennsylvania, 1982) p. 3.
30. M. G. SCHINKER, L. KÖNCZÖL and W. DÖLL, *J. Mat. Sci. Lett.* **1** (1982) 475.
31. J. C. MICHEL, PhD dissertation, Lehigh University (1984).
32. N. SATO, T. KURAUCHI, S. SATO and O. KAMIGAITO, *J. Mater. Sci. Lett.* **2** (1983) 188.
33. N. SATO, T. KURAUCHI, S. SATO and O. KAMIGAITO, *Proc. ACS Div. Polym. Mat. Sci. Engng.* **49** (1983) 124.
34. W. ELBER, ASTM STP 486 (American Society for Testing and Materials, Philadelphia, Pennsylvania, 1971) p. 230.
35. P. C. PARIS, R. J. BUCCI, E. T. WESSEL, W. G. CLARK and T. R. MAGER, ASTM STP 513 (American Society for Testing and Materials Philadelphia, Pennsylvania, 1972) p. 141.
36. R. W. HERTZBERG and E. F. J. VON EUW, *Int. J. Fract. Mech.* **7** (1971) 349.
37. K. MINAKAWA and A. J. McEVILY, *Scripta Metall.* **15** (1981) 633.
38. R. O. RITCHIE, in "Fatigue Thresholds", edited by J. Backlund, A. Blom and C. J. Beevers (EMAS, Warley, UK, 1981) p. 503.
39. R. O. RITCHIE and S. SURESH, *Metall. Trans.* **13A** (1982) 937.
40. G. T. GRAY, III, J. C. WILLIAMS and A. W. THOMPSON, *ibid.* **14A** (1983) 421.
41. R. W. LANG, *J. Mater. Sci. Lett.* **4** (1985) 1391.
42. H. L. COX, *Brit. J. Appl. Phys.* **3** (1952) 72.